PCCP

Accepted Manuscript

ROYAL SOCIETY OF CHEMISTRY

www.rsc.org/pccp

Journal Name

COMMUNICATION

Large-size nanosheets of 9,10-bis(phenylethynyl)anthrancene with high photoresponse and light emission anisotropy

Received 00th January 20xx,
Accepted 00th January 20xx

DOI: 10.1039/x0xx00000x

www.rsc.org/

Juan-Ye Wang,[ab] Hong-Dan Peng,[b] Jia-Mei Yang,[b] Jing-Hui Yan*[a] and Ge-Bo Pan*[b]

Large-size single crystalline nanosheets of 9,10-bis(phenylethynyl)-anthrancene were prepared by a facile solution process and fully characterized. Prototype photodetector was then fabricated on basis of a single nanosheet and exhibited superior performance with the largest photoresponse ratio up to ca. 10^5. Moreover, the nanosheets show obvious light emission anisotropy.

Organic multifunctional semiconductors have attracted a surge of interest because of their versatile properties in the active layers of nanodevices. Generally, multifunctional performance can be realized in single-component systems,[1,2] co-crystals,[3,4] and blend materials.[5,6] Noted that effective cocrystallization is often difficult to be achieved due to unpredictable change induced by the introduction of foreign components. Not just any two types of materials can recognize each other and form cocrystals.[3] Moreover, structural development is also complicated because phase separation and constituent crystallization could occur simultaneously in blend materials.[6] In comparison with cocrystals and blend materials, single-component systems are of particular interest due to their facile fabrication process and well-defined crystal structures. However, to the best our knowledge, only limited studies have been reported for single-component-based multifunctional properties.

Single crystalline, two-dimensional (2D) nanoscale structures with a large aspect ratio (the lateral extension compared to the thickness) are among the most appealing classes of organic multifunctional semiconductors.[7-9] Highly organized large-size 2D nanostructures combine the feature of both thin films with the large lateral dimension and single crystals with the high-level molecule ordering, allowing the fabrication of competent devices with ease.[10] The 2D organic crystal system is an ideal system to study the optical and electronic properties.[10-13] However, compared to the extensive studies of 1D nanostructures, the investigations of large-size 2D nanostructures are exceptionally rare. This is possibly because of the obligation of weak intermolecular interactions. It remains a great challenge to prepare large-size 2D crystals since they are susceptible to disturbance by external factors.[11-12]

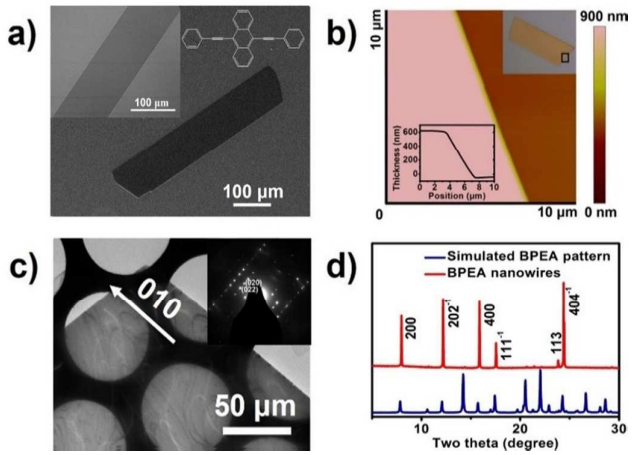

Fig. 1 (a) SEM, (b) AFM, and (c) TEM images of BPEA nanosheets. The inset of (a) is the chemical structure of BPEA molecule. The inset of (c) is an SEAD pattern recorded within a single nanosheet. (d) XRD pattern of nanosheets and simulated pattern from the single crystal data.

Herein, large-size nanosheets of 9,10-bis(phenylethynyl)anthrancene (BPEA, Fig. 1) with smooth surface were fabricated by a facile solution process. BPEA molecule, a typical π-conjugated system, has intrinsic planarity structure, which can facilitate molecular packing to obtain high-quality crystals. Importantly, BPEA is attractive candidate not only for its high charge transportability as organic semiconductor but also for unique fluorescent property and high emission efficiency.[14-17] The nanosheets were directly used for the fabrication of prototype photodetectors. The devices exhibited high performance and were highly reproducible under the white light illumination. The largest photoresponse ratio (i.e. I_{light}/I_{dark}) was up to 10^5. Moreover, the high-level molecular organization endues the BPEA nanosheets with light emission anisotropy.

[a] College of Chemistry and Environmental Engineering, Changchun University of Science and Technology, 130022 Changchun, China. E-mail: yjh@cust.edu.cn.
[b] Suzhou Institute of Nano-tech and Nano-bionics, Chinese Academy of Sciences, 215123 Suzhou, P. R. China. E-mail: gbpan2008@sinano.ac.cn.

† Electronic Supplementary Information (ESI) available: [Experimental section, single crystal structure, FTIR and UV-Vis spectra, and transfer characteristics. See DOI: 10.1039/x0xx00000x

In a typical synthesis, BPEA powder was dissolved into dichloromethane at a concentration of 1.2 mg ml^{-1}. The solution was injected into isobutyl alcohol. The volume ratio of dichloromethane and isobutyl alcohol was 1:5. The mixed solution was shaken for 10 s and stored at room temperature for ~1 h. The final products were collected and washed with isobutyl alcohol several times. Then, a drop (~10 µl) of solution with dispersed BPEA nanosheets was deposited onto Si substrate. The solvent was allowed to evaporate completely in air and the resultant product was further annealed at 120 °C for 30 min.

Fig. 1a shows a representative scanning electron microscopy (SEM) image of the as-obtained sample. The image demonstrates the formation of nanosheet with smooth surface. The average width of nanosheets is 120 µm and the length is up to 500 µm. As shown in Fig. 1b, BPEA nanosheet thickness was measured using atomic force microscopy (AFM), and determined to be approximately 660 nm. In addition, the selected area electron diffraction (SEAD) pattern (the inset in Fig.1c) was consistent throughout the whole nanocrystal, corresponding to the single-crystalline nature of the nanosheet. The structure of BPEA nanosheet is investigated by the X-ray diffraction (XRD). Fig. 1d shows the XRD pattern of nanosheets and simulated pattern from the single crystal data[17]. The diffraction peaks in the XRD pattern of BPEA nanosheets can be indexed well as a monoclinic lattice. The lattice constants are a = 22.866, b = 5.3567, c = 16.930, β = 99.72°. The appearance of intense peaks indicate that the nanosheets formed at a fast anisotropic growth rate along the b-axis of crystal structure of BPEA (Fig. S1†).

Fourier-transform infrared (FTIR) spectra, as shown in Fig. S2a†, was measured to analyze the chemical composition of these nanosheets and possible structure change after fabrication. It is clear that the FT-IR spectrum of nanosheets has the same feature as that of the source powder of BPEA. This indicates that BPEA molecules do not undergo decomposition or other chemical reactions during the self-assembling process. Fig. S2b† shows typical UV-vis absorption spectra of nanosheets deposited on quartz and BPEA monomers in dichloromethane. The monomers exhibit two resolved absorption bands. It is noted that the bands of nanosheets are broadened in comparison with the two resolved bands of the monomers. Moreover, there is a red-shifting of the PL spectrum with respect to that of monomers resulting from the highly ordered molecule-packing in BPEA nanosheets.[15]

A prototype device is constructed to explore its photoresponse characteristics. Fig. 2a shows a schematic illustration of a nanosheet-based device. Finger electrodes with a length of 200 µm, width of 20 µm, and distance of 20 µm are fabricated by photolithography and electron beam deposition of Au on a Si substrate covered with 300 nm thick SiO_2. The nanosheets are fabricated at a volume ratio of dichloromethane and isobutyl alcohol of 1:5, which are similar to those shown in Fig. 1a. A drop (~10 µl) of isobutyl alcohol solution with dispersed nanosheets is dropped on the surface of Au electrodes and the solvent is allowed to evaporate in air. To remove the solvent thoroughly, the device is post-annealed at 120 °C for 30 min. Fig. 2b shows a typical optical image of an actual device. It can be seen that the nanosheet has been connected to the Au electrodes. Fig. 2c shows the typical I-V curves of the device in the dark and under the nanosheet has been connected to the Au electrodes. Fig. 2c shows the typical I-V curves of the device in the dark and under continuous

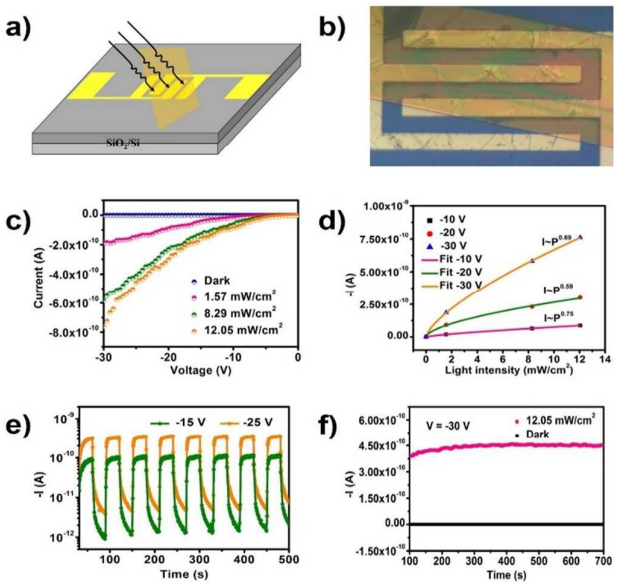

Fig. 2 (a) Schematic illustration and (b) representative optical image of the device based on a single BPEA nanosheets. (c) Dark current and photocurrents at different incident power densities. (d) Photocurrent versus incident optical densities measured at bias voltages of -5 V, -15 V and -25 V. (e) Time-dependent on/off switching of the device based on a single nanosheet. (f) Current versus time continuously over 600 s in dark and under illumination.

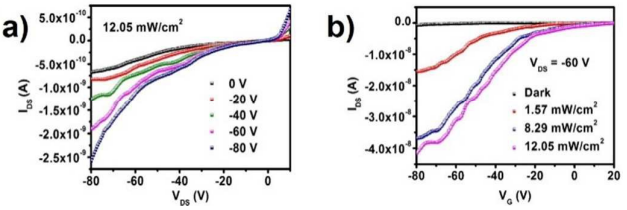

Fig. 3 (a) Output characterictics of a single BPEA nanosheet under illumination with 12.05 mW cm^{-2}. (b) Transfer characteristics of BPEA nanosheet in dark and under illumination at V_{DS} = -60V.

white light illumination. The slightly nonlinear curves indicate that there is a Schottky barrier at the contact between the nanosheet and Au electrodes. The photocurrent under light illumination is markedly higher than that obtained in the dark. At an applied bias of -30 V, the BPEA nanosheet in the dark shows a negligible current of 1.2 pA. At a low power density of 8.29 mW cm^{-2}, an electrical current of 583.1 pA is obtained. This corresponds to a photocurrent on/off ratio of ca. 485. The I_{light}/I_{dark} ratio is expected to be much larger if higher power illumination and/or longer electrode pairs are employed for the photocurrent measurement. At a high power density of 12.05 mW cm^{-2}, the photocurrent on/off ratio reaches 633, which is much higher than those of nanostructures of other anthracene derivatives. Such remarkable photoconductivity suggested that effective exciton dissociation occurred and photo-generated carriers migrated through nanosheet under a voltage bias.[18-20] The sensitivity of photocurrent to the intensity of the incident light may lie in different photon densities from the incident light. Fig. 2d shows the relationship

between photocurrent and incident light power densities. This can be well fitted to the power law $I_p \sim P^{\theta}$, where θ determines the response of the photocurrent to the light intensity. The fitting demonstrates a power dependence of ~0.75 at -10 V, 0.59 at -20 V, and 0.69 at -30 V, which is $I \sim P^{0.75}$, $I \sim P^{0.59}$ or $I \sim P^{0.69}$. The non-unity ($0.5 < \theta < 1$) exponent suggests a complex process of electron-hole generation, recombination, and trapping within a semiconductor.[21] The above characteristics indicate an excellent photo-capture in the BPEA nanosheet. On the basis of the active photosensitivity of the device based on BPEA nanosheet, the time-dependent photoresponse of the device is measured by periodically turning the white light on and off. Fig. 2e shows the typical on/off characteristics with the light turning on and off. The light power is 12.05 mW cm^{-2} and the applied voltages are -15 and -25 V. It is clear that the current of the device shows two distinct states, a "low" current state in the dark and a "high" current state under light illumination. The "on"- and "off"-state currents for 8 cycles remain almost the same and the switching in the two states is very fast and reversible. It is noted that the photocurrent durability and environmental stability of the photodetectors should also be highly valued in view of practical applications. As shown in Fig. 2f, the current in the dark nearly hold steady, while the photocurrent at -30 V starts to increase relatively slowly and finally remains almost steady. These results imply not only fast photosensitivity but also high stability of the device.

The excellent photoresponse characteristics may be attributed to the synergy effect of high charge transport and the surface morphology. X-ray crystallographic analysis showed the packing of BPEA crystals had a typical herringbone structure in the bc-plane. However, different from anthracene, the BPEA molecules have a strong co-facial π-π stacking owing to the side substitutions. There also exists aromatic C-H···π interaction between neighbouring molecules. Such a dense packing structure could significantly facilitate charge transport. On the other hand, surface morphology and lattice defects of the crystals heavily affect the performance of organic semiconductors devices because the conductive channels existing in several molecular layers on the surface and the defects may serve as carrier traps. Accordingly, the formed large size single-crystalline BPEA nanosheets have the flat surface and smallest possible number of defects, which is apt to achieve the high performance.

In comparison to photodiodes, organic phototransistors exhibited higher sensitivity and lower noise, besides optoelectronic integration of light detection and signal amplification in a single device. Fig. 3 shows the photoresponse behaviour of a phototransistor based on a single BPEA nanosheet in dark and under white light illumination. It was seen that the device showed typical p-type transporting behaviour and there was a large increase in current of I_{SD} under light illumination. Moreover, the current increased with the light intensity. This indicated that the output of the transistor could be controlled by both the incident light and the voltage. This result was similar to the diode characteristics. Note that the magnification of the current under illumination was more significant. The maximum I_{on}/I_{off} ratio of the phototransistor was over 10^5 at V_G = -8 V and V_{DS} = -40V with light power density of 12.05 mW cm^{-2} (Fig. S4†). The present performance is comparable or superior to other organic photo detectors based on polydopamine or perylene bisimide derivatives nanostructures.[22-24] Additionally, the photoresponsivity (R) based on the BPEA nanosheet was calculated as reported in the literature.[23] The R could reach 86.8 mW A^{-1} under illumination with light power density of 1.57 mW cm^{-2} at V_G = -80 V and V_{DS} = -60V. The high on/off ratio, together with the reversible and stable photoswitch characteristics, makes the BPEA nanosheets promising in highly sensitive photodetectors and photoswitches.

Considering the parallel conformation between the packed molecules, the anisotropy in the cross-section plane is expected to be small compared to the anisotropy along the π-π stacking.[25] Fig. 4 represents a typical rotating microscopy imaging of a nanosheet under crossed polarization, where the central image was taken in the bright field. When the nanostructure was nearly parallel to the direction of the polarizer, the birefringence of the nanosheet became minimal. Only when the nanosheet was aligned 45° to the transmission axis of either polarizers was the anisotropy birefringence maximized. These results imply that the optical axis is indeed along the direction of π-π stacking. In order to obtain further insight into the light emission anisotropy within the nanosheets, polarized photoluminescence emission is investigated.

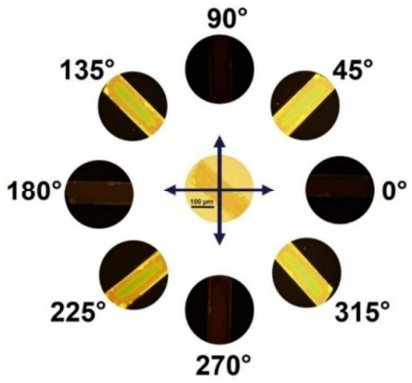

Fig. 4 A single nanosheet under cross-polarized microscope: successive rotation of the sample showed alternate appearance of maximum birefringence as the nanostructure was aligned 45° to either of the polarizers.

Fig. 5a and 5b show schematic illustration of polarized fluorescence emission measurements. The nanosheets were exited with a focused laser (405 nm) down to the diffraction at different excitation polarization angle. Normally, polarized emission is a direct consequence of the highly ordered alignment of organic molecules due to the intrinsic anisotropy of their electronic structure. BPEA has a demonstrated tendency to form anisotropic structure through π-π stacking during the self-assembly process. As expected, the emission intensity showed very strong dependence on the polarization and distribution function for the linear polarization in the crystal, which could be well fitted using a cosine squared function (Fig. 5c). It is clearly seen that the emission intensity detected with the parallel polarizer was much higher than that detected with the perpendicular polarizer. Such an observation implies the emission transition dipole moment is approximately along molecular stacking direction, as depicted in Fig. 5d. The above polarized light emission proves the

promising potential application of BPEA nanosheets in polarization-dependent nanophotonic devices.

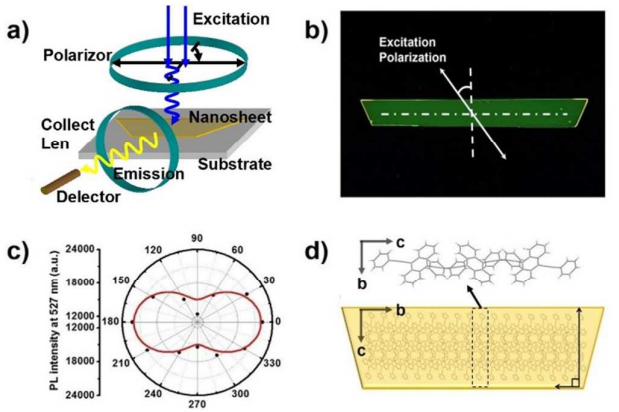

Fig. 5 (a) Schematic illustration of polarized fluorescence emission measurements under different angles of excitation polarization. (b) Relationship between the long axis of BPEA nanosheet and the excitation polarization. (c) Relationship between the PL intensity and the polarization angle. (d) Relationship between molecular stacking and the long axis direction in BPEA nanosheet.

In summary, large-size BPEA single-crystalline nanosheets with smooth surfaces were prepared via a facile solution process. The prototype photodetectors based on an individual nanosheet exhibited high photoresponse performance with the largest photoresponse ratio up to ca.10^5. Moreover, the rotating microscopy imaging and polarized PL spectra of BPEA nanosheets reveal typical characteristics of light emission anisotropy. All these studies should boost development of multifunctional properties of one material for potential applications in many fields in molecular electronic and photonics.

Acknowledgements

This work was supported by the National Natural Science Foundation of China (Nos. 21273272, 61404155), the China Postdoctoral Science Foundation (2013M541747), the Jiangsu Planned Projects for Postdoctoral Research Funds (1302159c), and the Chinese Academy of Sciences.

Notes and reference

1. Y. L. Guo, H. P. Zhao, G. Yu, C. A. Di, W. Liu, S. D. Jiang, S. K. Yan, C. R. Wang, H. L. Zhang, X. N. Sun, X. T. Tao, Y. Q. Liu, *Adv. Mater.*, 2008, **20**, 4835-4839.
2. W. L. Hu, Y. K. Chen, H. Jiang, J. G. Li, G. Zou, Q. J. Zhang, D. G. Zhang, P. Wang, H. Ming, *Adv. Mater.*, 2014, **26**, 3136-3141.
3. W. G. Zhu, R. H. Zheng, X. L. Fu, H. B. Fu, Q. Shi, Y. G. Zhen, H. L. Dong, and W. P. Hu, *Angew. Chem. Int. Ed.*, 2015, **54**, 6785-6789.
4. H. D. Wu, F. X. Wang, Y. Xiao and G. B. Pan, *J. Mater. Chem. C*, 2014, **2**, 2328-2332.
5. A. K. Blackburn, A. C. H. Sue, A. K. Shveyd, D. Cao, A. Tayi, A. Narayanan, B. S. Rolczynski, J. M. Szarko, O. A. Bozdemir, R. Wakabayashi, J. A. Lehrman, B. Kahr, L. X. Chen, M. S. Nassar, S. I. Stupp, and J. F. Stoddart, *J. Am. Chem. Soc.*, 2014, **136**, 17224-17235.
6. S. S. Lee, S. Muralidharan, A. R. Woll, M. A. Loth, Z. Li, J. E. Anthony, M. Haataja, and Y. L. Loo, *Chem. Mater.*, 2012, **24**, 2920-2928.
7. C. J. Park, M. S. Kim, J. Kim, J. Joo, *Syn. Mater.*, 2015, **199**, 394-399.
8. H. Jiang, K. K. Zhang, J. Ye, F. X. Wei, P. Hu, J. Guo, C. Y. Liang, X. D. Chen, Y. Zhao, Y. Zhao, L. E. McNeil, W. P. Hu, C. Kloc, *Small*, 2013, **7**, 990-995.
9. W. G. Zhu, Y. P. Yi, Y. G. Zhen, W. P. Hu, *Small*, 2015, **11**, 2150-2156.
10. M. B. Avinash, T. Govindaraju, *Adv. Funct. Mater.*, 2011, **21**, 3875-3882.
11. W. Yao, Y. L. Yan, L. Xue, C. Zhang, C. P. Li, Q. D. Zheng, Y. S. Zhao, H. Jiang, J. N. Yao, *Angew. Chem. Int. Ed.*, 2013, **52**, 8713-8717.
12. T. Govindaraju, M. B. Avinash, Nanoscale, 2012, 4, 6102-6117.
13. M. Han, T. Hirade, Chem. Commun., 2012, 48, 100-102.
14. M. Levitus, M. A. G. Garibay, J. Phys. Chem. A, 2000, 104, 8632-8637.
15. Y. S. Zhao, J. J. Xu, A. D. Peng, H. B. Fu, Y. Ma, L. Jiang, J. N. Yao, Angew. Chem. Int. Ed., 2008, 47, 7301-7305.
16. X. Z. Cai, D. Y. Ji, L. Jiang, G. Y. Zhao, J. H. Tan, G. F. Tian, J. Z. Li, W. P. Hu, Appl. Phys. Lett., 2014, 104, 063305.
17. C. L. Wang, Y. L. Liu, Z. Y. Ji, E. J. Wang, R. J. Li, H. Jiang, Q. X. Tang, H. X. Li, and W. P. Hu, Chem. Mater., 2009, 21, 2840-2845.
18. L. Jiang, Y. Y. Fu, H. X. Li, and W. P. Hu, *J. Am. Chem. Soc.*, 2008, **130**, 3937-3941.
19. X. H. Wang, S. F. Wang, L. Liu, M. W. Shao, and S. F. Li, *CrystEngComm.*, 2011, **13**, 5783-5787.
20. J. C. Xiao, Z. Y. Yin, B. Yang, Y. Liu, J. Guo, L. Huang, X. W. Liu, Q. Y. Yan, H. Zhang, and Q. C. Zhang, *Nanoscale*, 2011, **3**, 4720-4723.
21. L. Li, P. S. Lee, C. Y. Yan, T. Y. Zhai, X. S. Fang, M. Y. Liao, Y. Koide, Y. Bando, D. Golberg, *Adv. Mater.*, 2010, **22**, 5145-5149.
22. H. J. Nam, J. Cha, S. H. Lee, W. J. Yoo, and D. Y. Jung, *Chem. Commun.*, 2014, **50**, 1458-1461.
23. H. Yu, Z. N. Bao, and J. H. Oh, *Adv. Funct. Mater.*, 2013, **23**, 629-639.
24. B. Mukherjee, K. Sim, T. J. Shin, J. Lee, M. Mukherjee, M. Ree, and S. Pyo, *J. Mater. Chem.*, 2012, **22**, 3192-3200.
25. A. Datar, K. Balakrishnan, X. M. Yang, X. B. Zuo, J. L. Huang, R. Oitker, M. Yen, J. C. Zhao, D. M. Tiede, L. Zang, *J. Phys. Chem. B*, 2006, **110**, 12327-12332.